

A Statistical Dynamical Model to Predict Extreme Events and Anomalous Features in Shallow Water Waves with Abrupt Depth Change

Andrew J. Majda^{a,1}, M. N. J. Moore^b, and Di Qi^{a,1}

^aDepartment of Mathematics and Center for Atmosphere and Ocean Science, Courant Institute of Mathematical Sciences, New York University, New York, NY 10012;

^bDepartment of Mathematics and Geophysical Fluid Dynamics Institute, Florida State University, Tallahassee, FL

This manuscript was compiled on November 27, 2018

Understanding and predicting extreme events and their anomalous statistics in complex nonlinear systems is a grand challenge in climate, material, and neuroscience, as well as for engineering design. Recent laboratory experiments in weakly turbulent shallow water reveal a remarkable transition from Gaussian to anomalous behavior as surface waves cross an abrupt depth change (ADC). Downstream of the ADC, PDFs of surface displacement exhibit strong positive skewness, accompanied by an elevated level of extreme events. Here we develop a statistical dynamical model to explain and quantitatively predict the above anomalous statistical behavior as experimental control parameters are varied. The first step is to use incoming and outgoing truncated Korteweg-de Vries (TKdV) equations matched in time at the ADC. The TKdV equation is a Hamiltonian system which induces incoming and outgoing statistical Gibbs invariant measures. The statistical matching of the known nearly Gaussian incoming Gibbs state at the ADC completely determines the predicted anomalous outgoing Gibbs state, which can be calculated by a simple sampling algorithm, verified by direct numerical simulations, and successfully captures key features of the experiment. There is even an analytic formula for the anomalous outgoing skewness. The strategy here should be useful for predicting extreme anomalous statistical behavior in other dispersive media in different settings (21, 22).

extreme anomalous event | statistical TKdV model | matching Gibbs measures | surface wave displacement and slope

Understanding and predicting extreme events and their anomalous statistics in complex nonlinear systems is a grand challenge in climate, material and neuroscience as well as for engineering design. This is a very active contemporary topic in applied mathematics with qualitative and quantitative models (1–7) and novel numerical algorithms which overcome the curse of dimensionality for extreme event prediction in large complex systems (2, 8–11). The occurrence of Rogue waves as extreme events within different physical settings of deep water (12–16) and shallow water (17–19) is an important practical topic.

Recent laboratory experiments in weakly turbulent shallow water reveal a remarkable transition from Gaussian to anomalous behavior as surface waves cross an abrupt depth change (ADC). A normally-distributed incoming wave train, upstream of the ADC, transitions to a highly non-Gaussian outgoing wave train, downstream of the ADC, that exhibits large positive skewness of the surface height and more frequent extreme events (20). Here we develop a statistical dynamical model to explain and quantitatively predict this anomalous behavior as experimental control parameters are varied. The first step is to use incoming and outgoing truncated Korteweg-de Vries (TKdV) equations matched in time at the ADC. The TKdV

equation is a Hamiltonian system which induces incoming and outgoing Gibbs invariant measures. The statistical matching of the known nearly Gaussian incoming Gibbs state at the ADC completely determines the predicted anomalous outgoing Gibbs state, which can be calculated by a simple MCMC algorithm, verified by direct numerical simulations, and successfully captures key features of the experiment. There is even an analytic formula for the anomalous outgoing skewness. The strategy here should be useful for predicting extreme anomalous statistical behavior in other dispersive media in different settings (21, 22).

1. Experiments showing anomalous wave statistics induced by an abrupt depth change

Controlled laboratory experiments were carried out in (20) to examine the statistical behavior of surface waves crossing an ADC. In these experiments, nearly unidirectional waves are generated by a paddle wheel and propagate through a long, narrow wave tank. Midway through, the waves encounter a step in the bottom topography, and thus abruptly transition to a shallower depth. The paddle wheel is forced with a pseudo-random signal intended to mimic a Gaussian random sea upstream of the ADC. In particular, the paddle angle is

Significance Statement

Understanding and predicting extreme events and their anomalous statistics in complex nonlinear systems is a grand challenge in applied sciences as well as for engineering design. Recent controlled laboratory experiments in weakly turbulent shallow water with abrupt depth change exhibit a remarkable transition from nearly Gaussian statistics to extreme anomalous statistics with large positive skewness of the surface height. We develop a statistical dynamical model to explain and quantitatively predict the anomalous statistical behavior. The incoming and outgoing waves are modeled by the truncated Korteweg-de Vries equations statistically matched at the depth change. The statistical matching of the known nearly Gaussian incoming Gibbs state completely determines the predicted anomalous outgoing Gibbs state, and successfully captures key features of the experiment.

A.J.M. designed the research. A.J.M., M.N.J.M., and D.Q. performed the research. A.J.M., M.N.J.M., and D.Q. wrote the paper.

The authors declare no conflict of interest.

¹To whom correspondence should be addressed. E-mail: qidi@cims.nyu.edu, jonjon@cims.nyu.edu

125 specified as

$$126 \quad \theta(t) = \theta_0 + \Delta\theta \sum_{n=1}^N a_n \cos(\omega_n t + \delta_n), \quad E \sim (\Delta\theta)^2 \sum_n a_n^2 \omega_n^2.$$

129 where the weights a_n are Gaussian in spectral space with
 130 peak frequency ω_p and the phases δ_n are uniformly distributed
 131 random variables. The peak frequency gives rise to a char-
 132 acteristic wavelength λ_c which can be estimated from the
 133 dispersion relation. The energy E injected into the system
 134 is determined by the angle amplitude $\Delta\theta$, which is the main
 135 control parameter varied in (20). Optical measurements of the
 136 free surface reveal a number of surprising statistical features:
 137

- 138 • Distinct statistics are found between the incoming and
 139 outgoing wave disturbances: incoming waves display near-
 140 Gaussian statistics, while outgoing waves skew strongly
 141 towards positive displacement.
- 142 • The degree of non-Gaussianity present in the outgoing
 143 waves depends on the injected energy E : larger energies
 144 generate stronger skewness in the surface displacement
 145 PDFs and more extreme events.
- 146 • Compared to the incoming wave train, the power spectrum
 147 of the outgoing wave field decays more slowly, which
 148 indicates that the anomalous behavior is associated with
 149 an elevated level of high frequencies.

152 2. Surface wave turbulence modeled by truncated KdV 153 equation with depth dependence

154 The Korteweg-de Vries (KdV) equation is a one-dimensional,
 155 deterministic model capable of describing (weak?) surface
 156 wave turbulence. More specifically, KdV is leading-order
 157 approximation for surface waves governed by a balance of
 158 nonlinear and dispersive effects, valid in an appropriate far-
 159 field limit (23). Moreover, KdV has been adapted to describe
 160 waves propagating over variable depth (23). Here, we consider
 161 the variable-depth KdV equation truncated at wavenumber
 162 Λ (with $J = 2\Lambda + 1$ grid points) in order to generate weakly
 163 turbulent dynamics. The surface displacement is described
 164 by the state variable $u_\Lambda^\pm(x, t)$ with superscript ‘-’ for the
 165 incoming waves and ‘+’ for the outgoing waves. The Galerkin
 166 truncated variable $u_\Lambda = \sum_{1 \leq |k| \leq \Lambda} \hat{u}_k(t) e^{ikx}$ is normalized
 167 with zero mean $\hat{u}_0 = 0$ and unit energy $2\pi \sum_{k=1}^\Lambda |\hat{u}_k|^2 = 1$,
 168 which are conserved quantities. Here, $u_\Lambda \equiv \mathcal{P}_\Lambda u$ denotes the
 169 subspace projection. The evolution of u_Λ^\pm is governed by the
 170 truncated KdV equation with depth change D_\pm

$$171 \quad \frac{\partial u_\Lambda^\pm}{\partial t} + \frac{D_\pm^{-3/2}}{2} E_0^{1/2} L_0^{-3/2} \frac{\partial}{\partial x} \mathcal{P}_\Lambda (u_\Lambda^\pm)^2 + D_\pm^{1/2} L_0^{-3} \frac{\partial^3 u_\Lambda^\pm}{\partial x^3} = 0. \quad [1]$$

172 Equation [1] is non-dimensionalized on the periodic domain $x \in$
 173 $[-\pi, \pi]$. The depth is assumed to be unit $D_- = 1$ before the
 174 ADC and $D_+ < 1$ after the ADC. The conserved Hamiltonian
 175 can be decomposed as

$$176 \quad \mathcal{H}_\Lambda^\pm = D_\pm^{-3/2} E_0^{1/2} L_0^{-3/2} H_3(u_\Lambda^\pm) - D_\pm^{1/2} L_0^{-3} H_2(u_\Lambda^\pm),$$

$$177 \quad H_3(u) = \frac{1}{6} \int_{-\pi}^{\pi} u^3 dx, \quad H_2(u) = \frac{1}{2} \int_{-\pi}^{\pi} \left(\frac{\partial u}{\partial x} \right)^2 dx.$$

178 where we refer to H_3 as the cubic term and H_2 the quadratic
 179 term. We introduce parameters (E_0, L_0, Λ) based on the fol-
 180 lowing assumptions:

- 181 • The wavenumber truncation Λ is fixed at a moderate value for generating weakly turbulent dynamics. 187
 182 • The state variable u_Λ^\pm is normalized with zero mean and unit energy, $\mathcal{M}(u_\Lambda) = 0, \mathcal{E}(u_\Lambda) = 1$, which are conserved 188 during evolution. Meanwhile, E_0 characterizes the total 189 energy injected into the system based on the driving 190 amplitude $\Delta\theta$. 191
 192 • The length scale of the system L_0 is chosen so that the resolved scale $\Delta x = 2\pi L_0/J$ is comparable to the characteristic 193 wave length λ_c from the experiments. 194

195 Some intuition for how Eq. (1) produces different dynamics on either side of the ADC can be gained by considering the relative 196 contributions of H_3 and H_2 in the Hamiltonian \mathcal{H}_Λ^\pm . The depth 197 change, $D_+ < 1$, increases the weight of H_3 and decreases 198 that of H_2 , thereby promoting the effects of nonlinearity over dispersion and creating conditions favorable for extreme events. 199 Since $\frac{\partial u}{\partial x}$ is the slope of the wave height, $H_2(u)$ measures the 200 wave slope energy. 201
 202

203 A *deterministic matching condition* is applied to the surface 204 displacement u_Λ^\pm to link the incoming and outgoing wave trains. 205 Assuming the abrupt depth change is met at $t = T_{\text{ADC}}$, the 206 matching condition is given by 207

$$208 \quad u_\Lambda^-(x, t)|_{t=T_{\text{ADC}}-} = u_\Lambda^+(x, t)|_{t=T_{\text{ADC}}+},$$

209 Equation [1] is not designed to capture the short scale changes 210 in rapid time. Rather, since we are interested in modeling 211 statistics before and after the ADC, we will examine the long- 212 time dynamics of large-scale structures. 213

214 Interpreting experimental parameters in the dynamical model.

215 The model parameters (E_0, L_0, Λ) in [1] can be directly linked 216 to the basic scales from the physical problem. The important 217 characterizing parameters measured from the experiments 218 include: $\epsilon = \frac{a}{H_0}$ the wave amplitude a to water depth H_0 219 ratio; $\delta = \frac{H_0}{\lambda_c}$ the water depth to wavelength scale λ_c ratio; 220 and $D_0 = \frac{d}{H_0}$ the normalized wave depth ratio with incoming 221 flow depth $d = H_0$ to the outgoing flow depth $d < H_0$. The 222 interpretations and reference values of these model parameters 223 are based on the experimental setup (20). By comparing the 224 characteristic physical scales, the normalized TKdV equation 225 [1] can be linked directly with the measured non-dimensional 226 quantities by 227

$$228 \quad L_0 = 6^{\frac{1}{3}} \left(M \epsilon^{\frac{1}{2}} \delta^{-1} \right), \quad E_0 = \frac{27}{2} \gamma^{-2} \left(M \epsilon^{\frac{1}{2}} \delta^{-1} \right), \quad [2]$$

229 where M defines the computational domain size $M\lambda_c$ as M -
 230 multiple of the characteristic wavelength λ_c , and $\gamma = \frac{U}{a}$ represents 231 the factor to normalize the total energy in the state 232 variable u_Λ to one. 233

234 Consider the spatial discretization $J = 2\Lambda + 1$ so that the 235 smallest resolved scale is comparable with the characteristic 236 wavelength 237

$$238 \quad \Delta x = \frac{2\pi M \lambda_c}{J} \lesssim \lambda_c \Rightarrow M = \frac{J}{2\pi} \sim 5, \quad J = 32.$$

239 Therefore in the practical numerical simulations, we pick 240 $M = 5$ and γ varies in the range $[0.5, 1]$. Using the reference 241 experimental measurements (20), $\epsilon \in [0.0024, 0.024]$, $\delta \sim 0.22$, 242 and D_0 changes from 1 to 0.24 before and after the depth 243

249 change. The reference values for the model scales can be esti-
 250 mated in the range $L_0 \in [2, 6]$ and $E_0 \in [50, 200]$. These are
 251 the values we will test in the direct numerical simulations. See
 252 details about the derivation from scale analysis in *SI Appendix*,
 253 A.

254

255 3. Equilibrium statistical mechanics for generating the 256 stationary invariant measure

257 Since the TKdV equation satisfies the Liouville property, the
 258 equilibrium invariant measure can be described by an equi-
 259 librium statistical formulism (24–26) using a Gibbs measure
 260 with the conserved energy \mathcal{E}_Λ and Hamiltonian \mathcal{H}_Λ . The equi-
 261 librium invariant measure is dictated by the conservation laws
 262 in the TKdV equation. In the case with fixed total energy E_0 ,
 263 this is the *mixed Gibbs measure* in the truncated model with
 264 microcanonical energy and canonical Hamiltonian ensembles
 265 (24)

266
$$\mathcal{G}_\theta^\pm(u_\Lambda^\pm; E_0) = C_\theta^\pm \exp(-\theta^\pm \mathcal{H}(u_\Lambda^\pm)) \delta(\mathcal{E}(u_\Lambda^\pm) - E_0), \quad [3]$$

267 with θ representing the “inverse temperature”. The distinct
 268 statistics in the upstream and downstream waves can be con-
 269 trolled by the value of θ . Negative temperature, $\theta^\pm < 0$, is
 270 the appropriate regime to predict the experiments as shown
 271 below. In the incoming flow field, the inverse temperature θ^-
 272 is chosen so that \mathcal{G}_θ^- has Gaussian statistics. Using the above
 273 invariant measures [3], the expectation of any functional $F(u)$
 274 can be computed based on the Gibbs measure

275
$$\langle F \rangle_{\mathcal{G}_\theta} \equiv \int F(u) \mathcal{G}_\theta(u) du.$$

276 The value of θ in the invariant measure is specified from $\langle H_\Lambda \rangle_{\mathcal{G}_\theta}$
 277 (24, 26). The invariant measure also predicts an equilibrium
 278 energy spectrum without running the TKdV equation directly.
 279 On the other hand, the time autocorrelation and transient
 280 statistics about the state variable u_Λ cannot be recovered from
 281 the statistical theory.

282 **Statistical matching condition in invariant measures before
 283 and after the abrupt depth change.** The Gibbs measures \mathcal{G}_θ^\pm
 284 are defined based on the different inverse temperatures θ^\pm on
 285 the two sides of the solutions

286
$$\begin{aligned} \mu_t^-(u_\Lambda^-; D_-), \quad u_\Lambda |_{t=T_{ADC}-} &= u_0, \quad t < T_{ADC}; \\ \mu_t^+(u_\Lambda^+; D_+), \quad u_\Lambda |_{t=T_{ADC}+} &= u_0, \quad t > T_{ADC}, \end{aligned}$$

287 where u_0 represents the deterministic matching condition be-
 288 tween the incoming and outgoing waves. The two distributions,
 289 μ_t^-, μ_t^+ should also be matched at the depth change location
 290 T_{ADC} , so that,

291
$$\mu_{t=T_{ADC}}^-(u_\Lambda) = \mu_{t=T_{ADC}}^+(u_\Lambda).$$

292 In matching the flow statistics before and after the abrupt
 293 depth change, we first use the conservation of the determinis-
 294 tic Hamiltonian H_Λ^+ after the depth change. Then assuming
 295 ergodicity (24, 25), the statistical expectation for the Hamil-
 296 tonian $\langle H_\Lambda^+ \rangle$ is conserved in time after the depth change at
 297 $t = T_{ADC}$ and should stay in the same value as the system ap-
 298 proaches equilibrium as $t \rightarrow \infty$. The final statistical matching
 299 condition to get the outgoing flow statistics with parameter
 300 θ^+ can be found by

301
$$\langle H_\Lambda^+ \rangle_{\mathcal{G}_\theta^+} = \langle H_\Lambda^+ \rangle_{\mathcal{G}_\theta^-}, \quad [4]$$

302 with the outgoing flow Hamiltonian H_Λ^+ and the Gibbs mea-
 303 sures \mathcal{G}_θ^\pm before and after the abrupt depth change.

304 4. The nearly Gaussian incoming statistical state

305 The incoming flow is always characterized by a near-Gaussian
 306 distribution in the wave displacement. It is found that a
 307 physically consistent Gibbs measure should take negative val-
 308 ues in the inverse temperature parameter $\theta < 0$, where a
 309 proper distribution function and a decaying energy spectrum
 310 are generated (see (26) and *SI Appendix*, B.1 for the explicit
 311 simulation results). The upstream Gibbs measure \mathcal{G}_θ^- with
 312 $D_- = 1$ displays a wide parameter regime in (θ^-, E_0) with
 313 near-Gaussian statistics. In the left panel of Figure 1 (a), the
 314 inflow skewness κ_3^- varies only slightly with changing values of
 315 E_0 and θ^- . The incoming flow PDF then can be determined
 316 by picking the proper parameter value θ^- in the near Gaus-
 317 sian regime with small skewness. In contrast, the downstream
 318 Gibbs measure \mathcal{G}_θ^+ with $D_+ = 0.24$ shown in the right panel
 319 of Figure 1 (a) generates much larger skewness κ_3^+ as the
 320 absolute value of θ^+ and the total energy level E_0 increases.
 321 The solid lines in Figure 1 (c) offer a further confirmation of
 322 the transition from near-Gaussian statistics with small κ_3^- to
 323 a strongly skewed distribution κ_3^+ after the depth change.

324 In the next step, the value of the downstream θ^+ is deter-
 325 mined based on the matching condition [4]. The expectation
 326 $\langle H_\Lambda^+ \rangle_{\mathcal{G}_\theta^-}$ about the incoming flow Gibbs measure can be cal-
 327 culated according to the predetermined parameter values of
 328 θ^- as well as E_0 from the previous step. For the direct nu-
 329 mercial experiments shown later in Figure 2, we pick proper
 330 choices of test parameter values as $L_0 = 6, E_0 = 100$ and
 331 $\theta^- = -0.1, -0.3, -0.5$. More test cases with different system
 332 energy E_0 can be found in *SI Appendix*, B.2 where similar
 333 transition from near Gaussian symmetric PDFs to skewed
 334 PDFs in the flow state u_Λ^\pm can always be observed.

335 **Direct numerical model simulations.** Besides the prediction of
 336 equilibrium statistical measures from the equilibrium statisti-
 337 cal approach, another way to predict the downstream model
 338 statistics is through running the dynamical model [1] directly.
 339 The TKdV equation is found to be ergodic with proper mixing
 340 property as measured by the decay of autocorrelations as long
 341 as the system starts from a negative inverse temperature state
 342 as described before. For direct numerical simulations of the
 343 TKdV equations, a proper symplectic integrator is required to
 344 guarantee the Hamiltonian and energy are conserved in time.
 345 It is crucial to use the symplectic scheme to guarantee the
 346 exact conservation of the energy and Hamiltonian since they
 347 are playing the central role in generating the invariant measure
 348 and the statistical matching. The symplectic schemes used
 349 here for the time integration of the equation is the 4th-order
 350 midpoint method (27). Details about the mixing properties
 351 from different initial states and the numerical algorithm are
 352 described in *SI Appendix*, C.

353 5. Predicting extreme anomalous behavior after the 354 ADC by statistical matching

355 With the inflow statistics well described and the numerical
 356 scheme set up, we are able to predict the downstream anomalous
 357 statistics starting from the near-Gaussian incoming flow
 358 going through the abrupt depth change from $D_- = 1$ to
 359 $D_+ = 0.24$.

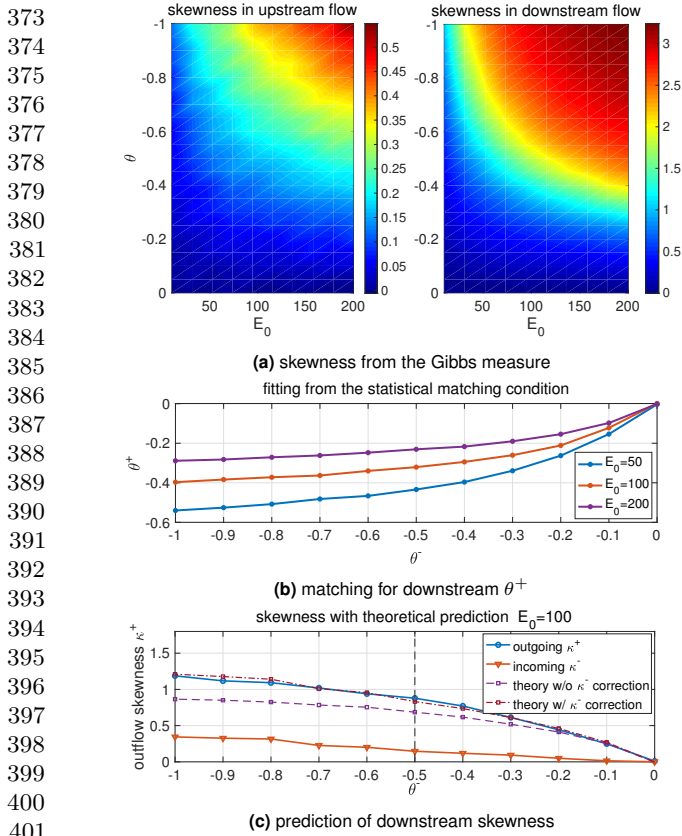


Fig. 1. First row: skewness from the Gibbs measures in incoming and outgoing flow states with different values of total energy E_0 and inverse temperature θ (notice the different scales in the incoming and outgoing flows); Second row: outgoing flow parameter θ^+ as a function of the incoming flow θ^- computed from the statistical matching condition with three energy level E_0 ; Last row: skewness in the outgoing flow with the matched value of θ^+ as a function of the inflow parameter θ^- (the theoretical predictions using [5] are compared).

$D_+ = 0.24$. First, we consider the statistical prediction in the downstream equilibrium measure directly from the matching condition. The downstream parameter value θ^+ is determined by solving the nonlinear equation [4] as a function of θ^+ , $F(\theta^+) = \langle H_\Lambda^+ \rangle_{\mathcal{G}_\theta^+}(\theta^+) - \langle H_\Lambda^+ \rangle_{\mathcal{G}_\theta^-} = 0$. In the numerical approach, we adopt a modified secant method avoiding the stiffness in the parameter regime (see the *SI Appendix, B.2* for the algorithm). The fitted solution is plotted in Figure 1 (b) as a function of the proposed inflow θ^- . A nonlinear $\theta^- - \theta^+$ relation is discovered from the matching condition. The downstream inverse temperature θ^+ will finally saturate at some level. The corresponding downstream skewness of the wave displacement u_Λ predicted from the statistical matching of Gibbs measures is plotted in Figure 1 (c). In general, a large positive skewness for outgoing flow κ_3^+ is predicted from the theory, while the incoming flow skewness κ_3^- is kept in a small value in a wide range of θ^- . Note that with $\theta^- \sim 0$ (that is, using the microcanonical ensemble only with energy conservation), the outflow statistics are also near Gaussian with weak skewness. The skewness in the outflow statistics grows as the inflow parameter value θ^- increases in amplitude.

For a second approach, we can use direct numerical simulations starting from the initial state sampled from the incoming flow Gibbs measure \mathcal{G}_θ^- and check the transient changes in the

model statistics. Figure 2 illustrates the change of statistics as the flow goes through the abrupt depth change. The first row plots the changes in the skewness and kurtosis for the state variable u_Λ after the depth change at $t = 0$. The PDFs in the incoming and outgoing flow states are compared with three different initial inverse temperatures θ^- . After the depth changes to $D_0 = 0.24$ abruptly at $t = 0$, both the skewness and kurtosis jump to a much larger value in a short time, implying the rapid transition to a highly skewed non-Gaussian statistical regime after the depth change. Further from Figure 2, different initial skewness (but all relatively small) is set due to the various values of θ^- . With small $\theta^- = -0.1$, the change in the skewness is not very obvious (see the second row of Figure 2 for the incoming and outgoing PDFs of u_Λ). In comparison, if the incoming flow starts from the initial parameter $\theta^- = -0.3$ and $\theta^- = -0.5$, much larger increase in the skewness is induced from the abrupt depth change. Furthermore, in the detailed plots in the third row of Figure 2 for the downstream PDFs under logarithmic scale, fat tails towards the positive direction can be observed, which represent the extreme events in the downstream flow (see also Figure 3 for the time-series of u_Λ).

As a result, the downstream statistics in final equilibrium predicted from the direct numerical simulations here agree with the equilibrium statistical mechanics prediction illustrated in Figure 1. The prediction from these two different approaches confirm each other.

6. Analytic formula for the upstream skewness after the ADC

A statistical link between the upstream and downstream energy spectra can be found for an analytical prediction of the skewness in the flow state u after the ADC. The skewness of the state variable u_j at one spatial grid point is defined as the ratio between the third and second moments

$$\kappa_3 = \langle u_j^3 \rangle_\mu / \langle u_j^2 \rangle_\mu^{3/2}.$$

Now we introduce mild assumptions on the distribution functions:

- The upstream equilibrium measure μ_- has a relatively small skewness so that

$$\langle H_3 \rangle_{\mu_-} = \frac{1}{6} \int_{-\pi}^{\pi} \langle u^3 \rangle_{\mu_-} dx \equiv \epsilon;$$

- The downstream equilibrium measure μ_+ is homogeneous at each physical grid point, so that the second and third moments are invariant at each grid point

$$\langle u_j^2 \rangle_{\mu_+} = \sigma^2 = \pi^{-1}, \quad \langle u_j^3 \rangle_{\mu_+} = \sigma^3 \kappa_3 = \pi^{-3/2} \kappa_3^+.$$

Then the skewness of the downstream state variable u_Λ^+ after the ADC is given by the difference between the inflow and outflow wave slope energy of u_x

$$\kappa_3^+ = \frac{3}{2} \pi^{1/2} L_0^{-3/2} E_0^{-1/2} D_+^2 \int_{-\pi}^{\pi} [\langle u_x^2 \rangle_{\mu_+} - \langle u_x^2 \rangle_{\mu_-}] dx + 3\pi^{1/2} \epsilon.$$

The detailed derivation is shown in *SI Appendix, B.2*. In particular, the downstream skewness with near-Gaussian inflow

497
498
499
500
501
502
503
504
505
506
507
508
509
510
511
512
513
514
515
516
517
518
519

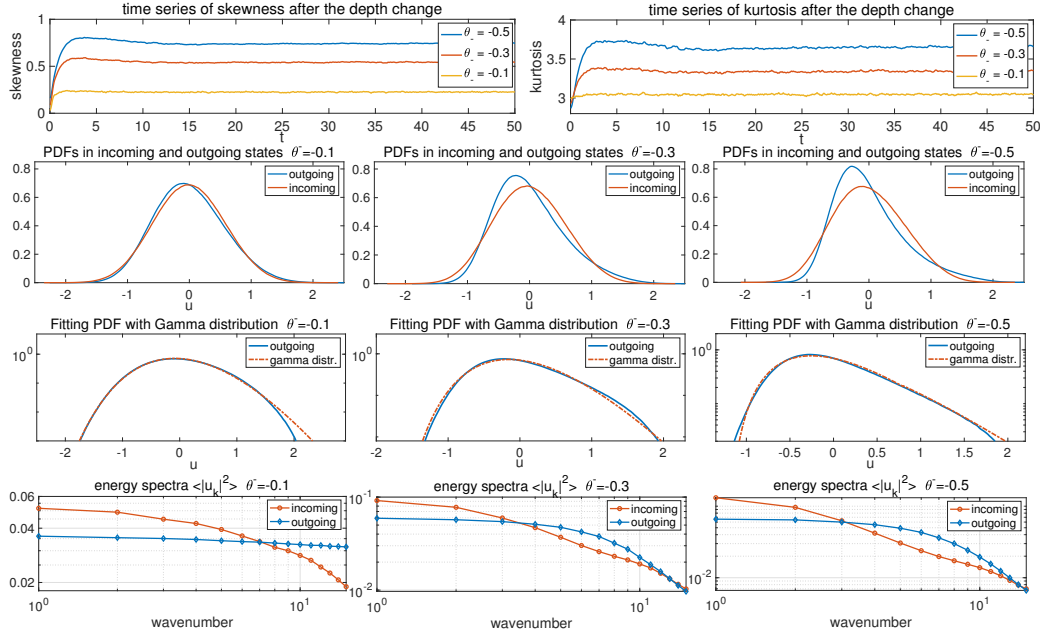


Fig. 2. Changes in the statistics of the flow state going through the abrupt depth change. The initial ensemble is set with the incoming flow Gibbs measure with different inverse temperature θ^- . First row: time evolution of the skewness and kurtosis. The abrupt depth change is taking place at $t = 0$; Second row: inflow and outflow PDFs of u_Λ ; Third row: the downstream PDFs fitted with Gamma distributions with consistent variance and skewness (in log coordinate in y); Last row: energy spectra in the incoming and outgoing flows.

523
524
525 statistics $\epsilon \ll 1$ is positive if and only if the difference of the
526 incoming and outgoing wave slope energy is positive. This
527 means that there is more small scale wave slope energy in the
528 outgoing state. As an evidence, in the last row of Figure 2
529 in all the weak and strong skewness cases, the outflow energy
530 spectrum always has a slower decay rate than the inflow energy
531 spectrum which possesses stronger energy in larger scales and
532 weaker energy in the smaller scales.

533 In Figure 1 (c), we compare the accuracy of the theoretical
534 estimation [5] with numerical tests. In the regime with small
535 incoming inverse temperature θ^- , the theoretical formula offers
536 a quite accurate approximation of the third-order skewness
537 using only information from the second-order moments of the
538 wave-slope spectrum.

539 **7. Key features from experiments captured by the sta-** 540 **tistical dynamical model**

541 In this final section, we emphasize the crucial features generated
542 by the statistical dynamical model [1] by making comparison
543 with the experimental observations in (20). As from the scale analysis displayed in Section 2, the theory is set in
544 the same parameter regime as the experimental setup.

- 545 • The transition from near-Gaussian to skewed non-
546 Gaussian distribution as well as the jump in both skewness
547 and kurtosis observed in the experiment observations (Fig.
548 1 of (20)) can be characterized by the statistical model
549 simulation results (see the first and second row of Figure
550 2). Notice that the difference in the decay of third and
551 fourth moments in the far end of the downstream regime
552 from the experimental data is due to the dissipation effect
553 in the flow from the wave absorbers that is not mod-
554 eled in the statistical model here. The model simulation
555 time-series plotted in Figure 3 can be compared with

556 the observed time sequences from experiments (Fig. 1 of
557 (20)). The downstream simulation generates waves with
558 strong and frequent intermittency towards the positive
559 displacement, while the upstream waves show symmetric
560 displacements in two directions with at most small peaks
561 in slow time. Even in the time-series at a single location
562 $x = 0$, the long-time variation displays similar structures.

- 563 • The downstream PDFs in experimental data are estimated
564 with a Gamma distribution in Fig. 2 of (20). Here in
565 the same way, we can fit the highly skewed outgoing
566 flow PDFs from the numerical results with the Gamma
567 distribution

$$\rho(u; k, \alpha) = \frac{e^{-k} \alpha^{-1}}{\Gamma(k)} (k + \alpha^{-1} u)^{k-1} e^{-\alpha^{-1} u}.$$

568 The parameters (k, α) in the Gamma distribution are fit-
569 ted according to the measured statistics in skewness and
570 variance, that is, $\sigma^2 = k\alpha^2$, $\kappa_3 = 2/\sqrt{k}$. And the excess
571 kurtosis of the Gamma distribution can be recovered as
572 $\kappa_4 = 6/k$. As shown in the third row of Figure 2, excellent
573 agreement in the PDFs with the Gamma distributions is
574 reached in consistency with the experimental data obser-
575 vations. The accuracy with this approximation increases
576 as the initial inverse temperature θ^- increases in value to
577 generate more skewed distribution functions.

- 578 • Experimental measurements of the power spectra (Fig. 4
579 of (20)) reveal the downstream measurements to contain
580 more energy at small scales, i.e. a relatively slower decay
581 rate of the spectrum. This result is also observed in the
582 direct numerical simulations here (detailed results shown
583 in *SI Appendix, C.2*), as the outgoing state contains more
584 energetic high frequencies.

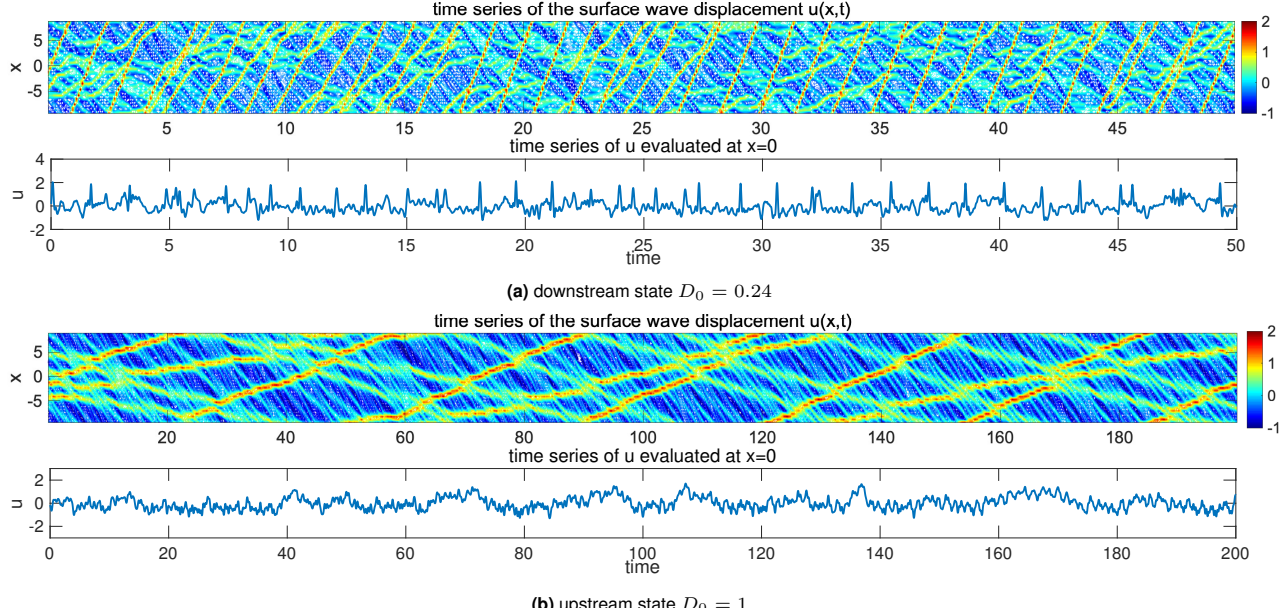


Fig. 3. Realization of the downstream and upstream flow solutions u_A^\pm . Note the larger vertical scale in the downstream time-series plot.

8. Concluding discussion

We have developed a statistical dynamical model to explain and predict extreme events and anomalous features of shallow water waves crossing an abrupt depth change. The theory is based on the dynamical modeling strategy consisting of the TKdV equation matched at the abrupt depth change with conservation of energy and Hamiltonian. Predictions can be made of the extreme events and anomalous features by matching incoming and outgoing statistical Gibbs measures before and after the abrupt depth transition. The statistical matching of the known nearly Gaussian incoming Gibbs state completely

determines the predicted anomalous outgoing Gibbs state, which can be calculated by a simple sampling algorithm, verified by direct numerical simulations, and successfully captures key features of the experiment. An analytic formula for the anomalous outgoing skewness is also derived. The strategy here should be useful for predicting extreme statistical events in other dispersive media in different settings.

ACKNOWLEDGMENTS. This research of A. J. M. is partially supported by the Office of Naval Research through MURI N00014-16-1-2161. D. Q. is supported as a postdoctoral fellow on the second grant. M.N.J.M would like to acknowledge support from Simons grant 524259.

1. Majda AJ, Branicki M (2012) Lessons in uncertainty quantification for turbulent dynamical systems. *Discrete & Continuous Dynamical Systems-A* 32(9):3133–3221.
2. Mohamad MA, Sapsis TP (2018) A sequential sampling strategy for extreme event statistics in nonlinear dynamical systems. *Proceedings of the National Academy of Sciences* 115(44):11138–11143.
3. Qi D, Majda AJ (2016) Predicting fat-tailed intermittent probability distributions in passive scalar turbulence with imperfect models through empirical information theory. *Communications in Mathematical Sciences* 14(6):1687–1722.
4. Majda AJ, Tong XT (2015) Intermittency in turbulent diffusion models with a mean gradient. *Nonlinearity* 28(11):4171–4208.
5. Majda AJ, Chen N (2018) Model error, information barriers, state estimation and prediction in complex multiscale systems. *Entropy* 20(9):644.
6. Majda AJ, Tong XT (2018) Simple nonlinear models with rigorous extreme events and heavy tails. *arXiv preprint arXiv:1805.05615*.
7. Thual S, Majda AJ, Chen N, Stechmann SN (2016) Simple stochastic model for el nino with westerly wind bursts. *Proceedings of the National Academy of Sciences* 113(37):10245–10250.
8. Chen N, Majda AJ (2018) Efficient statistically accurate algorithms for the Fokker-Planck equation in large dimensions. *Journal of Computational Physics* 354:242–268.
9. Chen N, Majda AJ (2017) Beating the curse of dimension with accurate statistics for the Fokker-Planck equation in complex turbulent systems. *Proceedings of the National Academy of Sciences* 114(49):12864–12869.
10. Chen N, Majda AJ (2018) Conditional Gaussian systems for multiscale nonlinear stochastic systems: Prediction, state estimation and uncertainty quantification. *Entropy* 20(7):509.
11. Qi D, Majda AJ (2018) Predicting extreme events for passive scalar turbulence in two-layer baroclinic flows through reduced-order stochastic models. *Communications in Mathematical Sciences* 16(1):17–51.
12. Adcock TA, Taylor PH (2014) The physics of anomalous ('rogue') ocean waves. *Reports on Progress in Physics* 77(10):105901.
13. Cousins W, Sapsis TP (2015) Unsteady evolution of localized unidirectional deep-water wave groups. *Physical Review E* 91(6):063204.
14. Farazmand M, Sapsis TP (2017) Reduced-order prediction of rogue waves in two-dimensional deep-water waves. *Journal of Computational Physics* 340:418–434.
15. Onorato M, Osborne AR, Serio M, Bertone S (2001) Freak waves in random oceanic sea states. *Physical Review Letters* 86(25):5831–5834.
16. Demattei G, Grafke T, Vanden-Eijnden E (2018) Rogue waves and large deviations in deep sea. *Proceedings of the National Academy of Sciences* 115(5):855–860.
17. Sergeeva A, Pelinovsky E, Talipova T (2011) Nonlinear random wave field in shallow water: variable Korteweg-de Vries framework. *Natural Hazards and Earth System Sciences* 11(2):323–330.
18. Trulsen K, Zeng H, Gramstad O (2012) Laboratory evidence of freak waves provoked by non-uniform bathymetry. *Physics of Fluids* 24(9):097101.
19. Viotti C, Dias F (2014) Extreme waves induced by strong depth transitions: Fully nonlinear results. *Physics of Fluids* 26(5):051705.
20. Bolles CT, Speer K, Moore MNJ (2018) Anomalous wave statistics induced by abrupt depth change. *arXiv preprint arXiv:1808.07958*.
21. Solli D, Ropers C, Koopath P, Jalali B (2007) Optical rogue waves. *Nature* 450(7172):1054.
22. Höhmann R, Kuhl U, Stöckmann HJ, Kaplan L, Heller E (2010) Freak waves in the linear regime: A microwave study. *Physical review letters* 104(9):093901.
23. Johnson RS (1997) *A modern introduction to the mathematical theory of water waves*. (Cambridge university press) Vol. 19.
24. Abramov RV, Kovačič G, Majda AJ (2003) Hamiltonian structure and statistically relevant conserved quantities for the truncated Burgers-Hopf equation. *Communications on Pure and Applied Mathematics: A Journal Issued by the Courant Institute of Mathematical Sciences* 56(1):1–46.
25. Majda A, Wang X (2006) *Nonlinear dynamics and statistical theories for basic geophysical flows*. (Cambridge University Press).
26. Bajars J, Frank J, Leimkuhler B (2013) Weakly coupled heat bath models for Gibbs-like invariant states in nonlinear wave equations. *Nonlinearity* 26(7):1945–1973.
27. McLachlan R (1993) Symplectic integration of hamiltonian wave equations. *Numerische Mathematik* 66(1):465–492.